IEEE Access
Multidisciplinary | Rapid Review | Open Access Journal

SPECIAL SECTION ON ADVANCED ENERGY STORAGE TECHNOLOGIES AND THEIR APPLICATIONS

Received September 13, 2018, accepted October 3, 2018, date of publication October 17, 2018, date of current version November 14, 2018.

Digital Object Identifier 10.1109/ACCESS.2018.2876095

An Integrated Energy Management Strategy With Parameter Match Method for Plug-In Hybrid Electric Vehicles

CHUN WANG[1,2], BO HUANG[2], AND WENNA XU[2]

[1]State Key Laboratory of Automotive Simulation and Control, Changchun 130012, China
[2]School of Mechanical Engineering and Sichuan Provincial Key Lab of Process Equipment and Control, Sichuan University of Science and Engineering, Zigong 643000, China

Corresponding author: Chun Wang (susewangchun@163.com)

This work was supported in part by the Foundation of State Key Laboratory of Automotive Simulation and Control under Grant 20161102, in part by the Foundation of Sichuan Provincial Department of Education under Grant 17ZB0307, in part by the Foundation of Sichuan Provincial Key Lab of Process Equipment and Control under Grant GK201705, and in part by the Talent Project of Sichuan University of Science and Engineering under Grant 2017RCL42.

ABSTRACT A battery-ultracapacitor hybrid energy storage system (HESS) is a reliable candidate to overcome the drawbacks of a single power source system for its complementary features of power and energy in plug-in hybrid electric vehicle application. In this paper, an integrated energy management strategy procedure, which consists of three layers, is presented to distribute the power of the battery packs and the ultracapacitor packs. First, an HESS parameter match method is developed under different driving cycles with optimization objectives of cost and weight. Second, three-level wavelet transform (WT) algorithm is employed to isolate the different frequency components of power demand. The low-frequency components with less transients and sharps in power demand are provided by extending the battery lifetime, while an ultracapacitor satisfies the high-frequency components for its nice features of high specific power. Finally, fuzzy logic control is used to manage power flows between various components for guaranteeing the HESS performance. The simulation results show that compared with WT-based-only energy management strategy, the proposed procedure can always control the battery currents within 2C rate and reduce the energy consumption of about 6.54%.

INDEX TERMS Integrated energy management strategy, wavelet transform, fuzzy logic control, parameter match, hybrid energy storage system, plug-in electric vehicles, ultracapacitor.

I. INTRODUCTION

Plug-in hybrid electric vehicle (PHEV) is seen as one of the most promising technologies to deal with global warming and dependence on fossil fuels, recently [1], [2]. Compared with pure electric vehicles (EV), PHEV has a greater electrically propulsion distance with lighter energy storage system (ESS) and longer service lifetime [3], [4]. However, when the PHEV is in starting, braking and accelerating situations, battery-only ESS cannot provide both power and energy requirements without damage the internal electrochemical structure of batteries [5]. Therefore, hybrid energy storage system (HESS) is implemented as one of the most reliable candidates to satisfy the mutually exclusive attributes required between power and energy. Many energy storage systems are introduced in the previous literatures. It is typically divided into three categories: mechanical energy storage systems, electrical energy storage systems and chemical energy storage systems. Furthermore, the fuel cell, compressed air and battery have slow response times while the ultracapacitor, flywheel and superconducting magnetic have fast response times. The battery, fuel cell and ultracapacitor are the typical energy storage systems that have received many attentions from renewable energy system and smart grid arenas. However, the appropriate topologies of HESSs are required to coordinate the power distribution among different energy storage systems. Although many combinations of HESSs have been proposed and analyzed in the literatures, the battery-ultracapacitor HESS is employed in this paper [6]. The reason is that batteries possess high specific energy that can largely determine the propulsion distance, while ultracapacitors have a nice feature

of high specific power to satisfy the power requirements on acceleration, starting and braking situations.

A combination of battery and ultracapacitor and a suitable energy management strategy can extend the battery lifetime by alleviating the stress of battery current load. Generally, the energy management strategies not only limit battery currents within a suitable rate but also control ultracapacitor to absorb short-time peak currents. Many energy management strategies have reported in the literatures [7]. The rule-based energy management strategy is mainly cooperated with other optimization methods such as dynamic programming (DP) algorithm. For example, the optimized control rules are extracted among different driving cycles by DP, and the optimal control effects under specific operating condition are obtained [8], [9]. Wang *et al.* [10] developed a Markov model to predict the power demand for improving the fuzzy logic control (FLC) effects. According to a detailed analysis of historical data, Zhou *et al.* [11] presented an adaptive membership function. In addition, Yi *et al.* [12] proposed a combination energy management strategy including FLC and machine learning method to improve the control performance. Shen and Khaligh [13] trained the neural network model by DP optimized parameters for online-controlling of battery-ultracapacitor HESS. To observe the battery aging track, Song *et al.* [14] built a battery degradation model implementing in HESS. Gomozov *et al.* [15] employed non-uniform sampling times for realizing model predictive control under different conditions to reduce the calculating burden. Recently, with the rapid development of artificial intelligence (AI) algorithms, the reinforcement learning algorithm has been applied in energy management field [16]. Liu *et al.* [17] proposed a reinforcement learning-based adaptive energy management, and the results show that the method has nice adaptability, optimality and learning ability. However, in spite of the above mentioned energy management strategies can deal with the issues of HESS optimization control in many aspects, the transients and sharps in power demand, which can damage the battery internal electrochemical structure and shorten battery lifetime, were not fully considered. Therefore, researchers proposed a frequency-based filtering algorithm to isolate the low and high frequency components while these components are provided by battery and ultracapacitor, respectively. Nonetheless, the constant debugging process to approach the ideal filter effect is a serious computational burden [18].

In the HESSs, the wavelet transform (WT) algorithm is selected to play a role aiming to avoid the rapid variation and peak in power demand [19], [20]. The WT has a nice feature that decomposes a time domain signal into different frequency groups by a scalable modulated time window of varying size [21], [22]. Since the WT algorithm shows excellent performance in comprehending the time and frequency information simultaneously, it is employed to capture the transients in power demand such as the driving cycles of a vehicular system [23], [24]. The FLC methodology has been proven that it is an effective way to obtain certain and reliable results from imprecise information, which is essentially a type of rule-based control method. The establishment of FLC does not require a definite mathematical model while its robustness and precision are strongly dependent on the researcher's experience [25]. In order to improve the effectiveness of HESS, a FLC considering battery and ultracapacitor (State of Charge) SOCs is applied in dealing with power distribution either. In addition, the parameters of HESS are strongly related to the PHEV performance. Namely, the series and parallel structure of battery and ultracapacitor largely determines the characteristics of HESS [26]. Thus, the HESS parameter match method should be integrated into energy management strategy.

Consequently, this paper develops an energy management strategy procedure consisting of three steps. Firstly, a HESS parameter match method is introduced in details to determine an optimal HESS configuration with reasonable consideration of overall cost and weight. Secondly, the WT algorithm splits the low and high frequency power demand directly. Finally, the FLC strategy distributes these components by considering the natural features of power sources to guarantee the energy management performance.

This paper is organized as follows. Section II describes the HESS parameter match method in details. Section III presents the energy management strategy based on WT and fuzzy logic control. In Section IV, the results of developed energy management strategy are evaluated and verified. Finally, conclusions are given in Section V.

II. HESS PARAMETER MATCH METHOD

The object of HESS parameter match method is to ensure vehicles' power performance with an optimized combination between battery and ultracapacitor. The HESS parameter match method consists of three steps. First, the primary parameters of the PHEV and the key indicators of six typical driving cycles are analyzed in details. Second, the energy and power requirements are systematically discussed to calculate the thresholds of the HESS. Finally, the HESS optimized parameters are obtained with the optimization objectives of HESS cost and weight.

A. ANALYSIS OF DIFFERENT DRIVING CYCLES

In HESSs for PHEV, battery is the main energy supply system, and ultracapacitor is the main power supply system. The dynamical model of PHEV can be shown as following

$$P_{\text{req}} = \frac{1}{\eta}\left(\frac{Mgf\cos(\beta)}{3600}v_{\text{a}} + \frac{Mg\sin(\beta)}{3600}v_{\text{a}} + \frac{C_{\text{D}}A}{76140}v_{\text{a}}^3 + \frac{\delta M}{3600}\frac{dv_{\text{a}}}{dt}\right) \quad (1)$$

where, P_{req} is power requirement, v_{a} represents the vehicle velocity and β denotes the grade of the road. In addition, the corresponding parameters of the PHEV are listed as Table 1.

The standard driving cycle can reflect the vehicle running status actually. The power and energy requirements are determined by characteristic parameters of driving cycle

TABLE 1. The primary parameters of the PHEV.

Parameters	Values
η - Efficiency of the transmission system	0.9
M - Curb weight	1845 kg
g - Gravitational acceleration	9.8 m/s^2
f - Rolling resistance coefficient	0.025
C_D - Air resistance coefficient	0.36
A - Windward area	2.53 m^2
δ - Correction coefficient of the rotation mass	1.03
Maximum speed	≥130 km/h
Acceleration time for 0~50 km/h	≤10 s
Acceleration time for 50~80 km/h	≤8 s
Maximum climbing degree	≥25 %
Driving range	≥200 km
Assisting time	15 s
Motor voltage	360 V

such as duration, driving range, average velocity, maximum acceleration and maximum velocity. Since each driving cycle has its individual characteristic parameters, in order to improve the suitability of parameter match results, the Highway Road (HWFET and INDIA_HWY), Suburb Road (CSHVR_Vehicle and WVUBUS) and Urban Road (MANHATTAN and NYCC) driving cycles are employed to analyze the power and energy requirements. The velocity and power curves of six standard driving cycles are shown in Fig. 1, and the characteristic parameters are listed as Table 2.

From Table 2, it can be seen that compared with highway road and urban road, the suburb road driving cycles have the longest duration. Specifically, the durations of CSHVR_Vehicle and WVUBUS correspondingly are 1781s and 1665s. Due to the frequent starting and stopping of PHEV, the MANHATTAN and HWFET have the shortest driving ranges of 3.3243 km and 1.8984 km, respectively. Moreover, the maximum acceleration of NYCC can be as high as 2.6822 m/s^2. The HWFET has the longest driving range, the maximum average velocity and the maximum velocity of 16.5061 km, 77.5744 km/h and 96.3971 km/h.

The power and energy requirements under different driving cycles can be summarized as Table 3. It can be observed that HWFET, INDIA_HWY and NYCC driving cycles have the larger positive peak power, which can reach to 41.2089 kW, 43.2945 kW and 44.4458 kW, respectively. Compared with other driving cycles, the HWFET driving cycle has the largest energy consumption of 12551 kJ. On the contrary, since the driving ranges are only about 11 km, the INDIA_HWY and WVUBUS driving cycles have energy consumptions of about 600 kJ. However, the energy consumption per km of HWFET reaches to 760 kJ and the value under other five driving cycles is only about 500 kJ. Since the frequent starting,

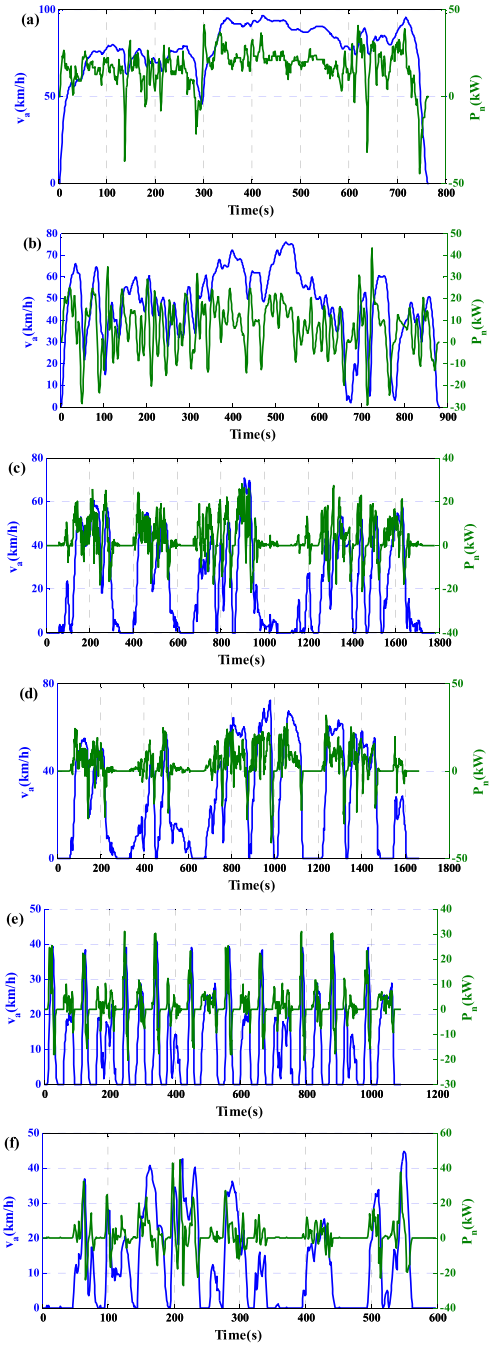

FIGURE 1. The velocity and power curves of six standard driving cycles. (a) HWFET; (b) INDIA_HWY; (c) CSHVR_Vehicle; (d) WVUBUS; (e) MANHATTAN; (f) NYCC.

acceleration and braking of PHEV in urban road, the ratios of positive energy requirement to negative energy requirement under MANHATTAN and NYCC correspondingly are 44.71 % and 45.56 %.

B. PARAMETER MATCH FOR ENERGY AND POWER REQUIREMENTS

1) BATTERY ENERGY REQUIREMENTS

In this paper, the battery is regarded as an ideal component and its efficiency is 100 %. If PHEV is driving at a constant

TABLE 2. The characteristic parameters of six standard driving cycles.

Type	Highway Road		Suburb Road		Urban Road	
Driving cycle	HWFET	INDIA	CSHVR	WVUBUS	MANHATTAN	NYCC
Duration (s)	766	882	1781	1665	1090	599
Driving range (km)	16.5061	11.6507	10.8139	11.9710	3.3243	1.8984
Average velocity (km/h)	77.5744	47.5540	21.8585	25.8833	10.9793	11.4094
Maximum acceleration (m/s^2)	1.4305	2.1210	1.1623	1.2949	2.0563	2.6822
Maximum velocity (km/h)	96.3971	76.0003	70.4873	72.1005	40.7153	44.5776

TABLE 3. The power and energy requirements under different driving cycles.

Type	Highway Road		Suburb Road		Urban Road	
Driving Cycle	HWFET	INDIA	CSHVR	WVUBUS	MANHATTAN	NYCC
Positive energy requirement（kJ）	13232.6014	7936.4519	7278.4101	7884.2473	2942.3874	1810.2138
Negative energy requirement（kJ）	-681.5105	-1894.9122	-2253.7733	-1974.4082	-1315.3963	-824.6439
Energy consumption（kJ）	12551.0909	6041.5397	5024.6368	5909.8391	1626.9911	985.5699
Energy consumption per km（kJ/km）	760.3911	518.5559	464.6461	493.6797	489.4237	519.1582
Positive power time（s）	699	642	1017	980	458	243
Negative power time（s）	61	237	379	266	238	146
Zero power time（s）	6	3	385	419	394	210
Positive average power（kW）	18.9308	12.3621	7.71567	8.0452	6.4244	7.4494
Negative average power（kW）	-11.1723	-7.9954	-5.9466	-7.4226	-5.5269	-5.6482
Positive peak power（kW）	41.2089	43.2945	28.0039	31.5243	30.9483	44.4458
Positive peak power（kW）	-44.6804	-28.9614	-21.6082	-41.3952	-20.3647	-27.2800

velocity of 60 km/h on the ideal road, the theoretical driving range is 200 km. Since the battery should satisfy the energy requirement for maximum theoretical driving range, which can be expressed as Eq. (2).

$$S = \frac{E_{200} v_a}{P_{req}} \tag{2}$$

where, S denotes the driving range, E_{200} represents the battery energy for 200 km, P_{req} is the power requirement for constant velocity and v_a denotes the constant velocity. The E_{200} can be easily calculated by Eq. (2) and the primary parameters of the PHEV are shown in Table 1. The safety factor of energy consumption is set to 1.2, and $E_{200} = 35$ kW.h. The battery energy can be expressed as Eq. (3).

$$E_{bat} = C_{bat} U_{bat} N_{bat,s} N_{bat,p} \tag{3}$$

where, C_{bat} is the battery cell capacity, U_{bat} denotes the nominal voltage of battery cell, $N_{bat,s}$ represents the battery number in series for each braches and $N_{bat,p}$ is the number of parallel braches. Thus, the first constraint equation can be obtained as following

$$C_{bat} \geq \frac{1000 E_{200}}{U_{bat} N_{bat,s} N_{bat,p}} \tag{4}$$

In this paper, the HESS includes a battery pack, an ultracapacitor pack and two bi-directional DC/DC converters. The efficiency of the DC/DC converter seriously affects the performance of the HESS. In addition, from Table 1, it can be seen that the motor voltage is 360 V. In order to keep the DC/DC converters in high efficiency working area, the battery pack voltage is set to 360 V as well. Thus, $N_{bat,s} \geq 100$.

2) ULTRACAPACITOR ENERGY REQUIREMENTS

The ultracapacitor is also considered an ideal component with efficiency of 100 % in this paper. The aim of ultracapacitor in HESS is to provide enough energy and power in the starting and acceleration status and absorb the braking energy in braking status.

a: PHEV STARTING

If PHEV start on the ideal road, the energy is only provided by ultracapacitor. The ultracapacitor energy should be no less than the maximum energy requirement for PHEV starting.

$$E_{\text{uc}} \geq E_{\text{start\_max}} = \int_0^t Fv(t)dt \tag{5}$$

where, E_{uc} denotes ultracapacitor energy requirement, $E_{\text{start\_max}}$ denotes the maximum energy requirement for PHEV starting. In general, the acceleration in the starting status reaches the maximum value. The maximum acceleration of NYCC is larger than that of other five driving cycles. Namely, if the ultracapacitor energy meets the maximum energy requirement for NYCC, it satisfies the requirement for other presented driving cycles as well. When PHEV accelerates to 50 km/h with an acceleration of 2.6822 m/s^2, the maximum ultracapacitor energy requirement is 0.049 kWh.

b: PHEV ACCELERATION

In the PHEV acceleration status, the HWFET has a maximum positive average power of 18.9308 kW and the MANHATTAN has a minimum positive average power of 6.4244 kW among the six driving cycles. In addition, the NYCC and CSHVR_Vehicle have the maximum and minimum positive peak power, respectively. The remaining power is defined as the difference between positive average power and positive peak power. In the energy management strategy, battery provides energy to meet the positive average power and ultracapacitor satisfies the remaining power. In addition, the maximum ultracapacitor energy requirement can be calculated as Eq. (6).

$$E_{\text{uc}} \geq E_{\text{ass\_max}} = \frac{1}{3600}\max\left(\int_0^t (P_{\text{ass\_peak}}(t) - P_{\text{avg}}(t))dt\right) \tag{6}$$

where, $E_{\text{ass\_max}}$ denotes the maximum energy requirement for PHEV acceleration, $P_{\text{ass\_peak}}$ and P_{avg} represent the positive peak power and positive average power of driving cycles, respectively. The assisting time t is set to 15s in this paper. Fig. 2 lists the ultracapacitor energy requirements under different driving cycles in acceleration status. It can be seen that compared with other driving cycles, the NYCC has a maximum ultracapacitor energy requirement of 0.1542 kWh.

c: PHEV BRAKING

In order to determine the maximum energy requirement for ultracapacitor in braking status, the ultracapacitor energy requirement should be no less than the maximum feedback

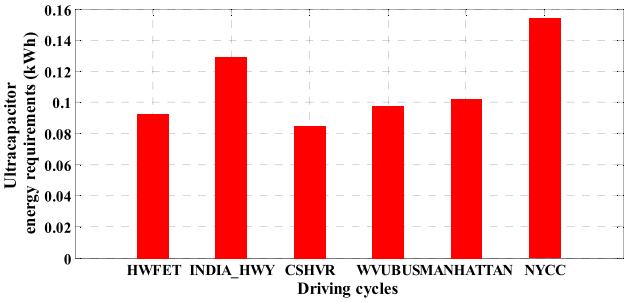

FIGURE 2. The ultracapacitor energy requirements under different driving cycles in acceleration status.

energy requirement among the six driving cycles. The maximum ultracapacitor energy requirement can be calculated as Eq. (7).

$$E_{\text{uc}} \geq E_{\text{reg\_max}} = \frac{1}{3600} \times \int_0^t P_{\text{reg}}(t)tdt \tag{7}$$

where, $E_{\text{reg\_max}}$ represents the maximum feedback energy requirement among the six driving cycles, P_{reg} denotes the negative peak power of driving cycles. The braking time t is set to 1s in this paper. Fig. 3 shows the ultracapacitor energy requirements under different driving cycles in braking status. It can be observed that compared with other driving cycles, the HWFET has a maximum ultracapacitor energy requirement of 0.01241 kWh.

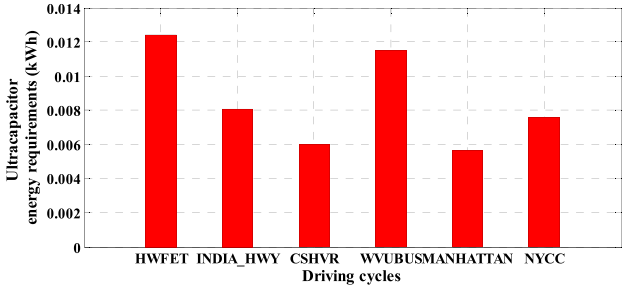

FIGURE 3. The ultracapacitor energy requirements under different driving cycles in braking status.

However, the ultracapacitor energy requirement E_{uc} is greater than the maximum value among $E_{\text{start}_{\text{m}}\text{ax}}$, $E_{\text{ass}_{\text{m}}\text{ax}}$ and $E_{\text{reg}_{\text{m}}\text{ax}}$. Thus, E_{uc} can be calculated by Eq. (8) and Eq. (9).

$$E_{\text{uc}} \geq \max(E_{\text{start\_max}}, E_{\text{ass\_max}}, E_{\text{reg\_max}}) \tag{8}$$

$$E_{\text{uc}} = \frac{1}{3600} \times \frac{1}{2} C_{\text{uc}} N_{\text{uc},s} N_{\text{uc},p} \left(U_{\text{cmax}}^2 - U_{\text{cmin}}^2\right) \tag{9}$$

where, C_{uc} is the rated capacity of ultracapacitor, U_{cmax} denotes the maximum ultracapacitor voltage of 2.7 V and U_{cmin} denotes the minimum ultracapacitor voltage of 1.35 V. $N_{\text{uc,s}}$ represents the battery number in series for each braches and $N_{\text{uc,p}}$ is the number of parallel braches. Therefore, the second constraint equation can be obtained as following

$$C_{\text{uc}} \geq \frac{3600 \times 2 \times 1000 \times \max\left(E_{\text{start\_max}}, E_{\text{ass\_max}}, E_{\text{reg\_max}}\right)}{N_{\text{uc,s}} N_{\text{uc,p}} \left(U_{\text{cmax}}^2 - U_{\text{cmin}}^2\right)} \tag{10}$$

Since the variation range of ultracapacitor voltage is much greater than that of battery voltage, the addition of DC/DC converter can stabilize the bus voltage of HESS. If the maximum ultracapacitor voltage is less than the minimum battery voltage, the DC/DC converter can be utilized more efficiently. Due to the battery SOC range is set to [0.2, 1.0] and the minimum battery voltage is about 270 V, the $N_{uc,s}$ is set to 100.

3) POWER REQUIREMENTS

The HESS power requirements should meet the maximum power among the six driving cycles. From Table 3, compared with other driving cycles, the NYCC has a maximum positive peak power of 44.4458 kW. Therefore, the third constraint equation can be obtained as following

$$P_{bat} + P_{uc} \geq P_{cyc\_max} \tag{11}$$

where, P_{bat} is battery power and P_{uc} denotes ultracapacitor power, which can be obtained as Eq.(12).

$$\begin{cases} P_{bat} = P_{avg} \\ P_{uc} = N_{uc,s} N_{uc,p} m_{uc,cell} s_{uc} \end{cases} \tag{12}$$

where, $m_{uc,cell}$ represents the ultracapacitor cell weight, s_{uc} is ultracapacitor power density. Since the surge current and large current can damage the internal electrochemical structure of batteries, the battery current is controlled within 2 C rate. In addition, the ultracapacitor will provide excessive current to ensure the power performance of PHEVs. Hence, the fourth constraint equation can be obtained as following

$$2 C_{bat} U_{bus} \geq P_{avg} \tag{13}$$

where, U_{bus} denotes the DC bus voltage which is set to 360 V, P_{avg} is the maximum positive average power among the six driving cycles. From Table 3, compared with other driving cycles, the HWFET has a maximum positive average power of 18.9308 kW [27].

4) PARAMETER MATCH METHOD

The different topologies of batteries and ultracapacitors lead to individual performance. According to the previous analysis, Eq. (4), (10), (11) and (13) are the constraint conditions of the parameter match method. Table 4 shows the capacity range of battery and ultracapacitor under different topologies.

The overall cost C_{hess} and weight M_{hess} of the HESS are the two optimization objectives and the battery capacity and ultracapacitor capacity are the optimization variables in this paper. In addition, the objective function is shown as following

$$\begin{cases} J(x) = \alpha C_{hess} + \beta M_{hess} \\ C_{hess} = N_{bat,s} N_{bat,p} m_{bat,cell} s_{bat} w_{bat} \\ \qquad\qquad + N_{uc,s} N_{uc,p} m_{uc,cell} s_{uc} w_{uc} \\ M_{hess} = N_{bat,s} N_{bat,p} m_{bat,cell} \\ \qquad\qquad + N_{uc,s} N_{uc,p} m_{uc,cell} \end{cases} \tag{14}$$

TABLE 4. The capacity ranges of battery and ultracapacitor under different topologies.

Numbers of battery parallel braches	Battery cell capacity (Ah)	Numbers of ultracapacitor parallel braches	Ultracapacitor cell capacity (F)
1	≥ 97.22	1	≥ 2030.62
2	≥ 48.61	2	≥ 1015.31
3	≥ 32.41	3	≥ 676.87
4	≥ 24.31	4	≥ 507.65

where, s_{bat} and s_{uc} are battery power density and ultracapacitor power density, respectively. w_{bat} denotes battery unit energy price which is 0.43 \$/Wh, and w_{uc} represents the ultracapacitor unit energy price of 11.55 \$/wh.$m_{bat,cell}$ represents the battery cell weight, and $m_{b\backslash uc,cell}$ represents the ultracapacitor cell weight. α and β are correspondingly the weight coefficients for cost and weight of HESS with a range of [0, 1]. In addition, the weight coefficients must satisfy $\alpha + \beta = 1$.

Considering the reliability and adaptability, the NMC lithium-ion battery with rated capacities of 25 Ah, 35 Ah, 60 Ah amd 100 Ah are selected in this paper. In addition, the selected ultracapacitor is supplied by Maxwell manufacturer, and the rated capacities are 650 F, 1500 F, 2000 F and 3000 F, respectively. The parameters of battery and ultracapacitor are correspondingly summarized as Table 5.

TABLE 5. The parameters of battery and ultracapacitor.

Battery			
C_{bat}(Ah)	$m_{bat,cell}$(kg)	s_{bat}(Wh/kg)	w_{bat}(\$/Wh)
25	0.585	170	0.43
35	1.08	135	0.43
60	1.85	130	0.43
100	3.05	115	0.43
Ultracapacitor			
C_{uc}(F)	C_{uc}(F)	C_{uc}(F)	C_{uc}(F)
650	650	650	650
1500	1500	1500	1500
2000	2000	2000	2000
3000	3000	3000	3000

The optimizing results of HESS parameters are shown as Fig. 4. If $\alpha = 0$ and $\beta = 1$, it shows that the weight M_{hess} is the only optimization objective. Point No.1 is the optimization result with $C_{hess} = 17.74$ k\$, $M_{hess} = 375$ kg, $N_{bat,p} = 1$ and $N_{uc,p} = 4$. From Table 4 and Table 5, the battery with a capacity of 100 Ah and the ultracapacitor with a capacity of 650 F are selected. On the contrary, If $\alpha = 1$ and $\beta = 0$, the cost C_{hess} is the only optimization objective. Point No.2 is the optimization result with $C_{hess} = 20.74$ k\$, $M_{hess} = 289$ kg, $N_{bat,p} = 4$ and $N_{uc,p} = 1$. The selected battery and ultracapacitor have capacities of 25 Ah and 3000 F, respectively. Considering the balance between cost C_{hess} and weight M_{hess},

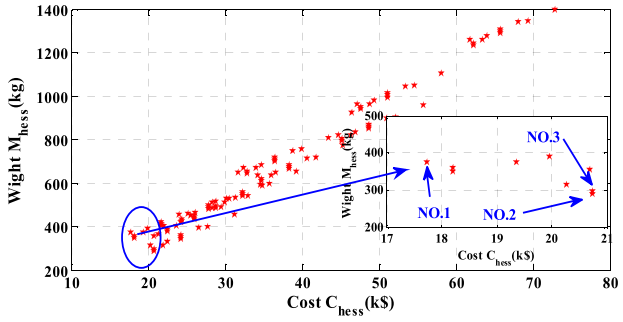

FIGURE 4. The optimizing results of HESS parameters.

α is set to 0.9 and β is set to 0.1, respectively. In this paper, point No.3 is the selected result with $C_{\text{hess}} = 20.74$ k\$, $M_{\text{hess}} = 298$ kg, $N_{\text{bat,p}} = 4$, $N_{\text{uc,p}} = 2$, battery capacity $C_{\text{bat}} = 25$ Ah and ultracapacitor capacity $C_{\text{uc}} = 1500$ F. Consequently, the configuration of HESS is $N_{\text{bat,s}} = 100$, $N_{\text{uc,s}} = 100$, $N_{\text{bat,p}} = 4$ and $N_{\text{uc,p}} = 2$.

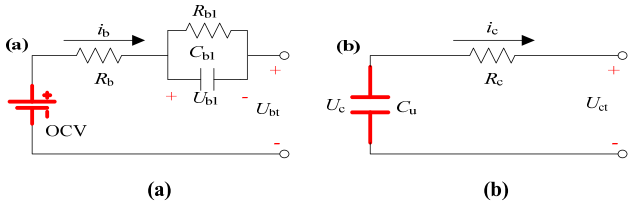

FIGURE 5. The equivalent circuit models for battery and ultracapacitor. (a) First-order RC model; (b) Rint model.

III. ENERGY MANAGEMENT STRATEGY BASED ON WAVELET TRANSFORM AND FUZZY LOGIC CONTROL

A. CONFIGURATION OF HESS

A battery-ultracapacitor HESS includes multiple topologies which are generally divided into fully active, semi-active and passive. In the HESS, the fully active topology is selected, which employs two bi-directional DC/DC converters to decouple the battery and ultracapacitor directly. As shown in Fig. 5, the first-order resistance-capacitance (RC) model and Rint model are selected for battery and ultracapacitor modeling, respectively. The model equations of battery and ultracapacitor are corresponding expressed as Eq. (15) and Eq. (16) [28], [29]. In order to accurately describe the dynamic characteristics of battery and ultracapacitor under different SOCs, the model parameters are identified by genetic algorithm (GA) and the parameters are shown in Fig. 6. From our previous research [30], to reduce the computational burden of modeling, a response surface $\xi(i_{\text{r}}, P_{\text{r}})$-based efficiency map shown in Table 6 is employed to simulate DC/DC converter efficiency. Additionally, i_{r} denotes output current and P_{r} represents the output power of DC/DC converter.

$$\begin{cases} \dot{U}_{\text{b1}} = -\frac{1}{C_{\text{b1}}R_{\text{b1}}}U_{\text{b1}} + \frac{1}{C_{\text{b1}}}i_{\text{b}} \\ U_{\text{bt}} = \text{OCV} - i_{\text{b}}R_{\text{b}} - U_{\text{b1}} \end{cases} \tag{15}$$

$$U_{\text{ct}} = U_{\text{c}} - i_{\text{c}}R_{\text{c}} \tag{16}$$

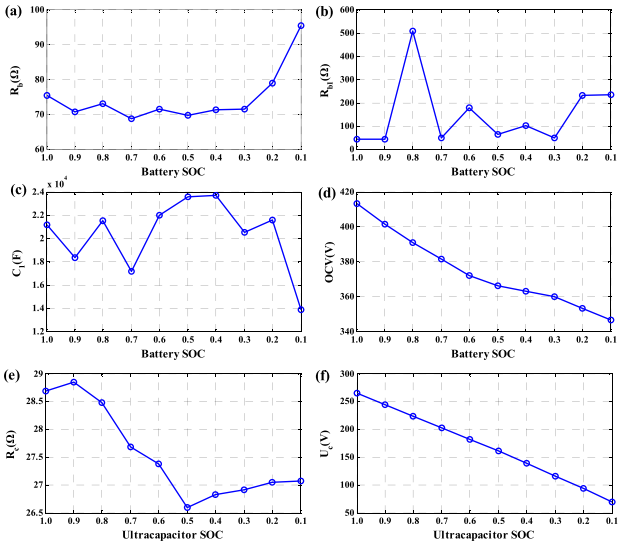

FIGURE 6. Identification parameters of battery and ultracapacitor. (a) ~ (d) battery parameters; (e) ~ (f) ultracapacitor parameters.

TABLE 6. The efficiency map of DC/DC converter.

$\xi(i_{\text{r}},P_{\text{r}})$	0kW	10kW	20kW	30kW	40kW	50kW	100kW
0 A	70%	70%	70%	70%	70%	70%	70%
10 A	70%	85%	88%	92%	90%	87%	84%
50 A	70%	89%	91%	94%	92%	88%	86%
100 A	70%	87%	90%	91%	88%	85%	83%
150 A	70%	80%	83%	87%	84%	82%	80%
300 A	70%	75%	75%	75%	75%	75%	75%

B. THEORY OF HAAR-WT AND FLC ALGORITHM

Owing to its shortest filter length and the simplest structure, Haar-wavelet is selected among different kinds of wavelets. In our previous study, a three-level Haar-wavelet transform shown as Fig. 7 is employed for the signal decomposing and reconstructing. A low pass filter $l_0(z)$ and a high pass filter $h_0(z)$ are used in the decomposition process and then a low pass synthesis filter $l_1(z)$ and a high pass synthesis filter $h_1(z)$ are used in the reconstruction process. Finally, the original signal $x(n)$ is reconstructed with very slight errors and the low and high frequency components of power demand are separated directly. It is well known that the critical issue of battery consists on reducing charging and discharging cycles in order to extend its lifetime, specially avoiding deep discharges as well as overcharges taking into account the SOC. In order to extend battery lifetime and take advantage of ultracapacitor, the battery will undertake the low frequency components and the ultracapacitor will satisfy the high frequency components. Due to the electric vehicle is a nonlinear of multivariable system and the exact mathematical model is difficult to establish, the FLC is quite suitable for

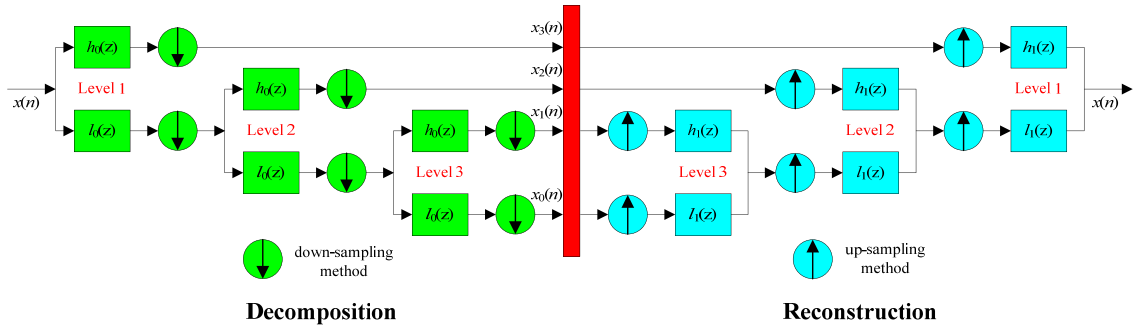

FIGURE 7. Three-level-Haar-WT decomposition and reconstruction.

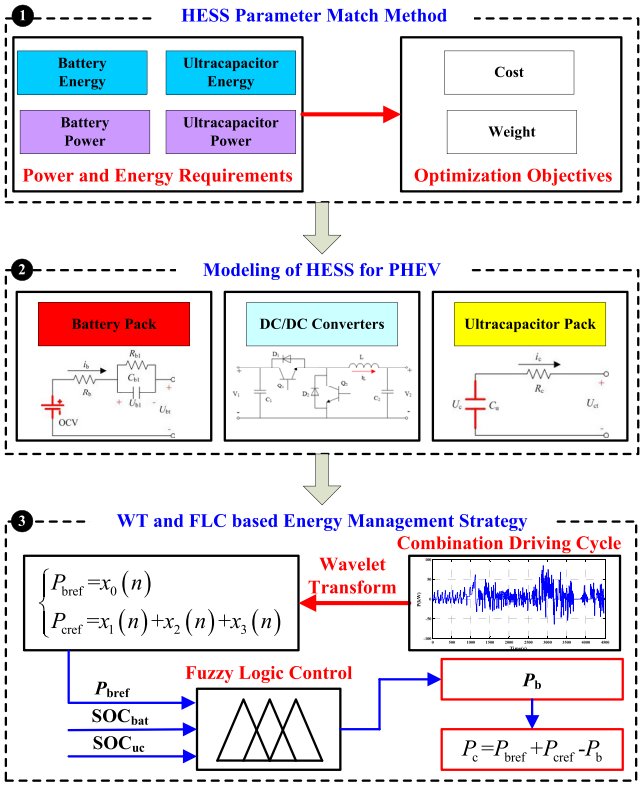

FIGURE 8. The structure of developed energy management based on WT and FLC.

HESS modeling with a higher level of abstraction originating based on the engineering experience. In this paper, multiple linear systems are employed for fitting nonlinear systems via Takagi-Sugeno controller. Since the structure of FLC is easy to implement and it has been widely and successfully used in various fields, we will not discuss the basic concept and principle in details.

C. ENERGY MANAGEMENT STRATEGY STRUCTURE

The structure of developed energy management based on WT and FLC is shown in Fig. 8. It can be seen that it composes of three steps: Modeling of HESS for PHEV and WT and FLC based energy management strategy. The first step and second step are correspondingly introduced in Section 2 and Section 3.1 in details while this section will discuss the

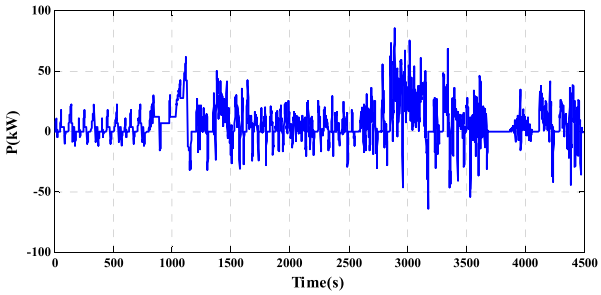

FIGURE 9. The load profile of combination driving cycle.

last step. Firstly, a comprehensive driving cycle consisting of NEDC, UDDS and UNIF01 driving cycles is developed to evaluate the dynamic response of HESS. The combination driving cycle shown in Fig. 9 is a 4486-s test procedure for reflecting different traffic conditions. Secondly, the wavelet transform can decompose the combination driving cycle into low and high frequency components. P_{bref} and P_{cref} denote the reference power demands for battery and ultracapacitor, respectively. Thirdly, in the HESS, the FLC has three input and one output variables. The inputs of FLC include the reference power demand for battery P_{bref}, the SOC values of battery SOC_{bat} and the SOC values of ultracapacitor SoC_{uc} while the output is the power demand for battery P_{b}. The SOC_{bat} and SoC_{uc} are set as [0, 1], and the values of P_{bref} is set as [−1, 1] by using the normalization tool. The fuzzy subset of SoC_{b} and SoC_{c} are divided into L, M, H, and the subsets of P_{bref} and P_{b} are divided into NH, NM, NL, Z, PL, PM, PH. In addition, the FLC consists of 63 rules designed by the engineering experience. Then P_{b} is obtained according to the anti-normalization tool. The membership functions of input and output variables are shown in Fig. 10. In addition, the power demand for ultracapacitor can be expressed as Eq. (17).

$$P_{\text{c}} = P_{\text{bref}} + P_{\text{cref}} - P_{\text{b}} \tag{17}$$

IV. SIMULATION AND VERIFICATION RESULTS

The simulation is implemented in MATLAB/Simulink platform which has many convenient toolboxes. In order to show the dynamic performances of WT and FLC based energy management strategy, the battery SOC, ultracapacitor SOC, battery current, ultracapacitor current, battery voltage, ultracapacitor voltage, battery output power and ultracapacitor

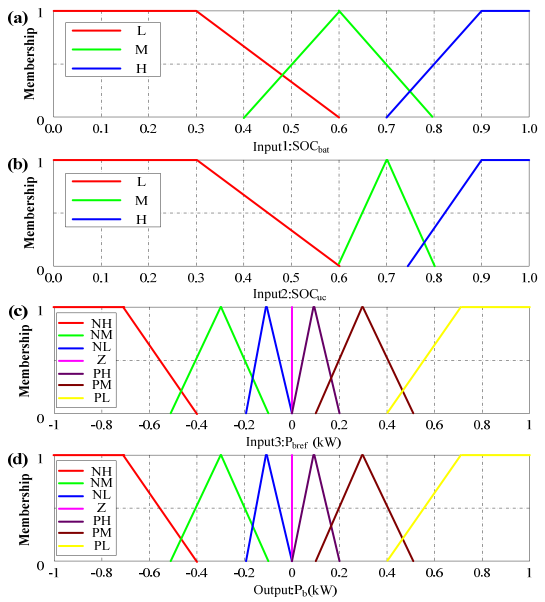

FIGURE 10. Membership functions of input and output variables.

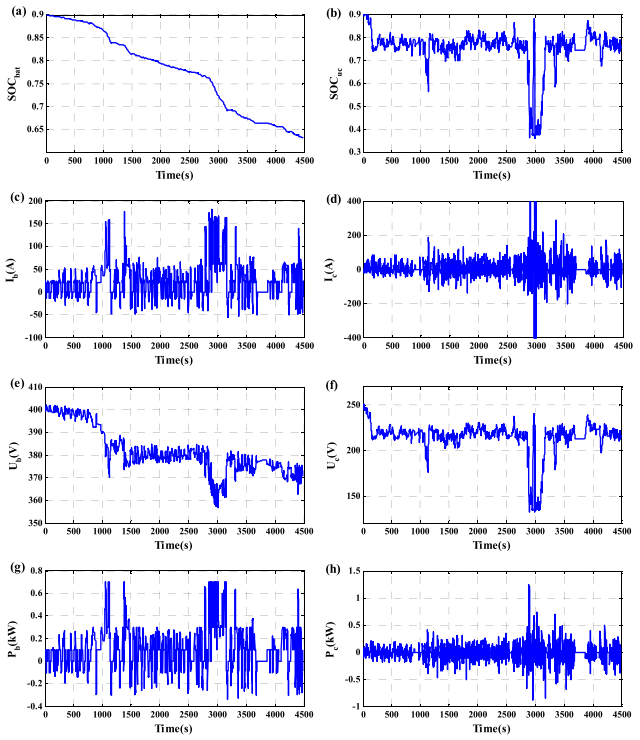

FIGURE 11. The evaluation results of WT and FLC based energy management strategy. (a) battery SOC; (b) ultracapacitor SOC; (c) battery current; (d) ultracapacitor current; (e) battery voltage; (f) ultracapacitor voltage; (g) battery output power; (h) ultracapacitor output power.

output power variation curves are demonstrated in Fig. 11. It is clear from Fig. 11(a), (c), (e) and (g) that the developed energy management strategy maintains the battery SOC within a reasonable level and the terminal battery SOC is 0.6324. The maximum battery current is only 181.86 A

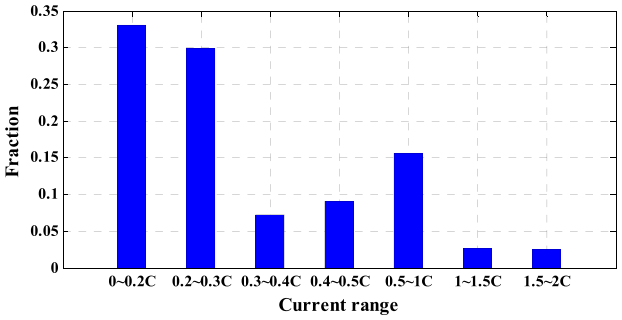

FIGURE 12. The battery current distribution on the combination driving cycle.

while it is successfully controlled to be within 2 C-rate. Additionally, the battery current distribution on the combination driving cycle is shown in Fig. 12. It is shown that the mainly battery currents are maintained within 0.5 C-rate while the proportion of battery currents over 1 C-rate is only 5.08 %. Therefore, it will greatly reduce the damage of battery electrochemical structure by sudden load variations and it is benefit for promoting battery lifetime. The variation of battery voltage is stable during the most of the driving cycle except for high accelerations and starting conditions. The battery continues to supply the steady power to satisfy the low frequency components of positive power demand and absorb the slow-variation negative portion. From Fig. 11(b), (d), (f) and (h), it is obvious that the ultracapacitor SOC has a wider variation range of [0.36, 0.93], and it changes more frequently compared to that of battery. The ultracapacitor can fulfill the power demand fluctuations owing to its fast response capability. Since the ultracapacitor power is close to zero at most of the time, the difference between initial and terminal ultracapacitor SOC is only 0.13. In addition, the maximum ultracapacitor current of 400 A and the frequent variations of ultracapacitor current and voltage prove that the transients and peak power demand are successfully absorbed by ultracapacitor. The WT and FLC based energy management strategy ensures that ultracapacitor has enough charge for accelerating periods while regulating the system power flow with the aim of decreasing energy consumption. Moreover, the WT-based-only energy management strategy without FLC provides an overall energy loss of 3936.72 kJ. It is shown that the adoption of FLC can improve an energy consumption of about 6.54 % under the developed energy management strategy.

V. CONCLUSIONS

In this research, a detailed study presents a WT and FLC based energy management procedure including an integration of HESS parameter match method for PHEV. The presented HESS parameter match method can optimize the HESS structure with reasonable and reliable balance between cost and weight. Then, a WT and FLC based energy management strategy focused on the reduction of transients and sharps of power demand for battery pack is proposed. The simulation results

reveal that compared with WT-based-only energy management strategy, the integrated energy management strategy is effective in reducing energy consumption of 6.54 %. Moreover, the overall battery currents during the combination driving cycle are maintained within 2 C-rate, and it benefits for alleviating the stress of battery and extend the battery lifetime. In the future, the integrated energy management strategy considering multi factors as well as the combination of multi control strategies to compensate for each own deficiencies are very attractive. In addition, the HESS is highly probable to be advanced by big data and machine learning.

ACKNOWLEDGMENT

The systemic experiments were performed at the Advanced Energy Storage and Application (AESA) Group, Beijing Institute of Technology.

REFERENCES

[1] P. Bubna, S. G. Advani, and A. K. Prasad, "Integration of batteries with ultracapacitors for a fuel cell hybrid transit bus," *J. Power Sources*, vol. 199, no. 1, pp. 360–366, 2012.

[2] P. Bajpai and V. Dash, "Hybrid renewable energy systems for power generation in stand-alone applications: A review," *Renew. Sustain. Energy Rev.*, vol. 16, no. 5, pp. 2926–2939, 2012.

[3] W. Sarwar, T. Engstrom, M. Marinescu, N. Green, N. Green, and G. J. Offer, "Experimental analysis of hybridised energy storage systems for automotive applications," *J. Power Sources*, vol. 324, pp. 388–401, Aug. 2016.

[4] R. Xiong, Y. Zhang, J. Wang, H. He, S. Peng, and M. Pecht, "Lithium-ion battery health prognosis based on a real battery management system used in electric vehicles," *IEEE Trans. Veh. Technol.*, to be published, doi: 10.1109/TVT.2018.2864688.

[5] M. Asghar, A. I. Bhatti, Q. Ahmed, and G. Murtaza, "Energy management strategy for Atkinson cycle engine based parallel hybrid electric vehicle," *IEEE Access*, vol. 6, pp. 28008–28018, 2018.

[6] Z. Chen, N. Guo, J. Shen, R. Xiao, and P. Dong, "A hierarchical energy management strategy for power-split plug-in hybrid electric vehicles considering velocity prediction," *IEEE Access*, vol. 6, pp. 33261–33274, 2018.

[7] R. Xiong, H. Chen, C. Wang, and F. Sun, "Towards a smarter hybrid energy storage system based on battery and ultracapacitor—A critical review on topology and energy management," *J. Cleaner Prod.*, vol. 202, pp. 1228–1240, Nov. 2018.

[8] S. Zhang, R. Xiong, and F. Sun, "Model predictive control for power management in a plug-in hybrid electric vehicle with a hybrid energy storage system," *Appl. Energy*, vol. 185, pp. 1654–1662, Jan. 2017.

[9] Z. Song, H. Hofmann, J. Li, X. Han, and M. Ouyang, "Optimization for a hybrid energy storage system in electric vehicles using dynamic programing approach," *Appl. Energy*, vol. 139, pp. 151–162, Feb. 2015.

[10] Y. Wang, W. Wang, Y. Zhao, L. Yang, and W. Chen, "A fuzzy-logic power management strategy based on Markov random prediction for hybrid energy storage systems," *Energies*, vol. 9, no. 1, p. 25, 2016.

[11] W. Zhou, M. Li, H. Yin, and C. Ma, "An adaptive fuzzy logic based energy management strategy for electric vehicles," in *Proc. IEEE 23rd Int. Symp. Ind. Electron.*, Jun. 2014, pp. 1778–1783.

[12] L. M. Yi, Z. Chen, L. Kiliaris, and M. A. Masrur, "Intelligent power management in a vehicular system with multiple power sources," *J. Power Sources*, vol. 196, no. 2, pp. 835–846, 2011.

[13] J. Shen and A. Khaligh, "A supervisory energy management control strategy in a battery/ultracapacitor hybrid energy storage system," *IEEE Trans. Transport. Electrific.*, vol. 1, no. 3, pp. 223–231, Oct. 2015.

[14] Z. Song, H. Hofmann, J. Li, J. Hou, X. Zhang, and M. Ouyang, "The optimization of a hybrid energy storage system at subzero temperatures: Energy management strategy design and battery heating requirement analysis," *Appl. Energy*, vol. 159, pp. 576–588, Dec. 2015.

[15] O. Gomozov, J. P. F. Trovão, X. Kestelyn, and M. R. Dubois, "Adaptive energy management system based on a real-time model predictive control with nonuniform sampling time for multiple energy storage electric vehicle," *IEEE Trans. Veh. Technol.*, vol. 66, no. 7, pp. 5520–5530, Jul. 2017.

[16] M. A. Hannan, M. S. H. Lipu, A. Hussain, M. H. Saad, and A. Ayob, "Neural network approach for estimating state of charge of lithium-ion battery using backtracking search algorithm," *IEEE Access*, vol. 6, pp. 10069–10079, 2018.

[17] T. Liu, Y. Zou, D. Liu, and F. Sun, "Reinforcement learning of adaptive energy management with transition probability for a hybrid electric tracked vehicle," *IEEE Trans. Ind. Electron.*, vol. 62, no. 12, pp. 7837–7846, Dec. 2015.

[18] Z. Song, H. Hofmann, J. Li, J. Hou, X. Han, and M. Ouyang, "Energy management strategies comparison for electric vehicles with hybrid energy storage system," *Appl. Energy*, vol. 134, pp. 321–331, Dec. 2014.

[19] Q. Li, W. Chen, Z. Liu, M. Li, and L. Ma, "Development of energy management system based on a power sharing strategy for a fuel cell-battery-supercapacitor hybrid tramway," *J. Power Sources*, vol. 279, pp. 267–280, Apr. 2015.

[20] O. Erdinc, B. Vural, and M. Uzunoglu, "A wavelet-fuzzy logic based energy management strategy for a fuel cell/battery/ultra-capacitor hybrid vehicular power system," *J. Power Sources*, vol. 194, no. 1, pp. 369–380, Oct. 2009.

[21] X. Zhang, C. C. Mi, A. Masrur, and D. Daniszewski, "Wavelet-transform-based power management of hybrid vehicles with multiple on-board energy sources including fuel cell, battery and ultracapacitor," *J. Power Sources*, vol. 185, no. 2, pp. 1533–1543, 2008.

[22] Y. Ates, O. Erdinc, M. Uzunoglu, and B. Vural, "Energy management of an FC/UC hybrid vehicular power system using a combined neural network-wavelet transform based strategy," *Int. J. Hydrogen Energy*, vol. 35, no. 2, pp. 774–783, Jan. 2010.

[23] M. Ibrahim, S. Jemei, G. Wimmer, N. Y. Steiner, C. C. Kokonendji, and D. Hissel, "Selection of mother wavelet and decomposition level for energy management in electrical vehicles including a fuel cell," *Int. J. Hydrogen Energy*, vol. 40, no. 45, pp. 15823–15833, 2015.

[24] M. Ibrahim, S. Jemei, G. Wimmer, and D. Hissel, "Nonlinear autoregressive neural network in an energy management strategy for battery/ultra-capacitor hybrid electrical vehicles," *Electr. Power Syst. Res.*, vol. 136, pp. 262–269, Jul. 2016.

[25] Q. Zhang and W. Deng, "An adaptive energy management system for electric vehicles based on driving cycle identification and wavelet transform," *Energies*, vol. 9, no. 5, p. 341, 2016.

[26] C. Zhang *et al.*, "Using CPE function to size capacitor storage for electric vehicles and quantifying battery degradation during different driving cycles," *Energies*, vol. 9, no. 11, p. 903, 2016.

[27] J. J. Hu *et al.*, "Control strategy and parameter optimization of hybrid energy storage device for electric vehicles," *J. Chongqing Univ.*, vol. 39, no. 1, pp. 1–11, 2016.

[28] C. Wang, H. He, Y. Zhang, and H. Mu, "A comparative study on the applicability of ultracapacitor models for electric vehicles under different temperatures," *Appl. Energy*, vol. 196, pp. 268–278, Jun. 2017.

[29] X. Hu, S. Li, and H. Peng, "A comparative study of equivalent circuit models for Li-ion batteries," *J. Power Sources*, vol. 198, pp. 359–367, Jan. 2012.

[30] C. Wang, R. Xiong, H. He, X. Ding, and W. Shen, "Efficiency analysis of a bidirectional DC/DC converter in a hybrid energy storage system for plug-in hybrid electric vehicles," *Appl. Energy*, vol. 183, pp. 612–622, Dec. 2016.

CHUN WANG was born in Zigong, Sichuan, China, in 1984. He received the B.S. degree in automation and the M.S. degree in mechatronic engineering from Xihua University, Chengdu, China, in 2006 and 2009, respectively, and the Ph.D. degree in mechanical engineering from the Beijing Institute of Technology and Collaborative Innovation Center of Electric Vehicles in Beijing, Beijing, China, in 2018.

Since 2010, he has been an Assistant Professor and then a Lecturer with the Sichuan University of Science and Engineering, Zigong.

His research interests mainly include electric vehicles, energy management strategy, and battery management systems.

BO HUANG was born in Neijiang, Sichuan, China, in 1978. He received the B.S. degree in mechanical engineering and automation from the Taiyuan University of Technology, Taiyuan, China, in 2002, and the M.S. degree in mechanical design and theory from the Sichuan University of Science and Engineering, Zigong, China, in 2013.

Since 2002, he was an Assistant Professor and then a Lecturer with the Sichuan University of Science and Engineering, Zigong, China.

His research interests mainly include mechanical design and manufacture, mechatronics, and embedded systems.

WENNA XU was born in Zigong, Sichuan, China, in 1987. She received the B.S. degree in industrial design and the M.S. degree in art from Xi'an Jiaotong University, Shaanxi, China, in 2010 and 2013, respectively.

Since 2013, she was an Assistant Professor and then a Lecturer with the Sichuan University of Science and Engineering, Zigong.

Her research interests mainly include ecological design, ergonomics, and interaction design.